IEEE Access
Multidisciplinary | Rapid Review | Open Access Journal

Received October 8, 2020, accepted October 16, 2020, date of publication October 20, 2020, date of current version October 30, 2020.

Digital Object Identifier 10.1109/ACCESS.2020.3032538

Bandgap Control of Two-Dimensional Coaxial Bragg Structures With Helically Corrugated Conductors

YING-XIN LAI[1], (Member, IEEE), XIAO-MIN JIANG[1], FANG-YUAN CHEN[2], JIAN LI[3], (Member, IEEE), AND TAI-JUN LIU[4], (Senior Member, IEEE)

[1]School of Electronic Engineering and Intelligentization, Dongguan University of Technology, Dongguan 523808, China
[2]Jinyichang Science and Technology Company Ltd., Jiaxing 314500, China
[3]School of Communication and Information Engineering, University of Electronic Science and Technology of China, Chengdu 610036, China
[4]Faculty of Electrical Engineering and Computer Science, Ningbo University, Ningbo 315211, China

Corresponding author: Ying-Xin Lai (yxlai@dgut.edu.cn)

This work was supported in part by the National Natural Science Foundation of China under Grant 61701116, Grant U1809203, and Grant 61771138; and in part by the Science and Technological Planning Project of Guangdong Province under Grant 2016A010101036.

ABSTRACT The untunable bandgap is a difficult problem for Bragg structures constructed from corrugated metallic waveguides, and becomes a major barrier for applications. Based on the coupled-mode theory, this paper presents the principle as well as a corresponding theoretical model of bandgap control of two-dimensional coaxial Bragg structures under the condition of a fixed ripple shape. It is shown that such control can be achieved by varying the angular deviation between the outer and inner corrugations, which can be done by rotating one of the conductors relative to the other. The effects of the proposed method on transmission bandgap control of two example structures were investigated by theoretical analysis and electromagnetic simulation. The results confirmed the validity of the proposal, and showed that such a control method can be used to manipulate the number and location of the working bands under multiple bandgap operation. These peculiarities provide potential applications of two-dimensional coaxial Bragg structures in constructing tunable passive and active high-power microwave devices.

INDEX TERMS Coaxial waveguides, Bragg gratings, bandgap, coupled mode analysis.

I. INTRODUCTION

In past decades, the use of periodic structures to manipulate the propagation of guided waves has been intensively investigated [1]–[4]. As a result of these efforts, many functional components using periodic structures have been proposed and then widely applied in the fields of radio frequency (RF) electronics, microwave electronics and optoelectronics. They include reflectors [5], filters [6]–[8], couplers [9], [10] and resonators [11]. In practice, periodic structures are implemented in various forms and materials to meet the needs of specific applications, with particular operating frequency bands and power capacities. For example, the periodic structures used in RF circuits and microwave devices are usually realized by etching periodic lattice structures on the conductive strip or ground plane of transmission lines [12], [13], or realized by waveguides with periodically arrayed membranes or nails [14]. In the optical systems, these structures are in the form of latticed crystals, multilayer films, dielectric materials with periodic refractive index [2], [4], [15], etc. Despite the differences of these structures, they all rely for their operation on Bragg scattering. This means that the periodic boundaries of the structures are able to scatter a forward wave coherently into a series of backward components, and the constructive interference of these scattered components opens up some so-called forbidden bands or stopbands in the frequency spectrum, where the propagation of the incident wave is strongly suppressed. Due to this characteristic, periodic structures are usually named Bragg structures [5]–[7], [11], electromagnetic bandgap (EBG) structures [8], [13], [16], and photonic bandgap (PBG) structures [4], [15], in different fields.

Bandgap parameters, such as the center frequency, amplitude and bandwidth, are generally the critical parameters

The associate editor coordinating the review of this manuscript and approving it for publication was Guido Valerio.

for determining the performance of periodic structures, and being able to controlling them is essential for many applications including microwave electronics, optics and signal processing [16]–[18]. Usually, the bandgap can be manipulated by changing the properties of the filling medium of the periodic structures. For the PBG structures used in optics, many techniques have been proposed to obtain the dynamic control of bandgap parameters by introducing different active media (for example Kerr-effect materials and chiral materials [18]–[20]) whose refractive indices can be manipulated by external stimuli such as electric fields or light. However, the Bragg structures used in microwave electronics, particularly in high-power microwave devices, have untunable bandgaps, which is a major drawback. The reason lies in the way they are constructed. The Bragg structures are planar or cylindrical metallic waveguides [5]–[7], [9], [11], where the periodicity is obtained by etching shallow periodic ripples on the internal surfaces of the conductor, and the filling medium (vacuum or air) is conformal with the ripples. The corrugation amplitude and period are fixed, so it is unrealistic to control the bandgap by changing the ripple shape. In order to improve their applicability, a new approach is required to manipulate bandgap parameters for Bragg structures with a fixed ripple shape.

Bragg structures with helical ripples have found increasing applications in constructing beam-wave interaction systems for gyro devices, and as the effective dispersive medium for pulse compressors [21]–[25]. Since the helical ripples have periodicities along the azimuthal and axial directions, they can be treated as two-dimensional periodic structures realized by metallic waveguides. Early investigations of two-dimensional Bragg structures mostly concentrated on structures with cylindrical topology. In recent years, growing attention has been paid to Bragg structures in the form of coaxial metallic waveguides, due to their merits in improving the performance of high-power free-electron devices [26]–[31]. It should be noted that, although the coupling coefficients and reflection characteristics of a two-dimensional coaxial Bragg structure with one or two helically corrugated conductors were investigated in [31], a method of manipulating the bandgap parameters of two dimensional coaxial Bragg structures is yet to be confirmed.

In this paper, the possibility of controlling the bandgap of two-dimensional coaxial Bragg structures with unchanged ripple shape is discussed as follows. In section II, the principle as well as the theoretical model of the bandgap control of two-dimensional coaxial Bragg structures is provided. Formulas are given for calculating the bandgap parameters and the means to manipulate the bandgap is provided. Control of the transmission bandgap of sample structures is demonstrated in section III. Finally, conclusions are drawn in section IV.

II. THEORETICAL MODEL AND PRINCIPLE OF BANDGAP CONTROL

A periodic function can be expanded to the superposition of different harmonics of sine/cosine functions. If the corrugation amplitude of periodic ripples is sufficiently small (less than 15% of the mean radius of the waveguide [25]), by neglecting the higher-order harmonics components, shallow periodic ripples with different shapes can be approximately expressed as sinusoidal/cosinusoidal ripples with certain amplitude [26]. In this section, we discuss bandgap control for two-dimensional coaxial Bragg structures with basic cosinusoidal ripples, where the principle and method are still applicable for two-dimensional coaxial Bragg structures corrugated with shallow periodic ripples of other shapes.

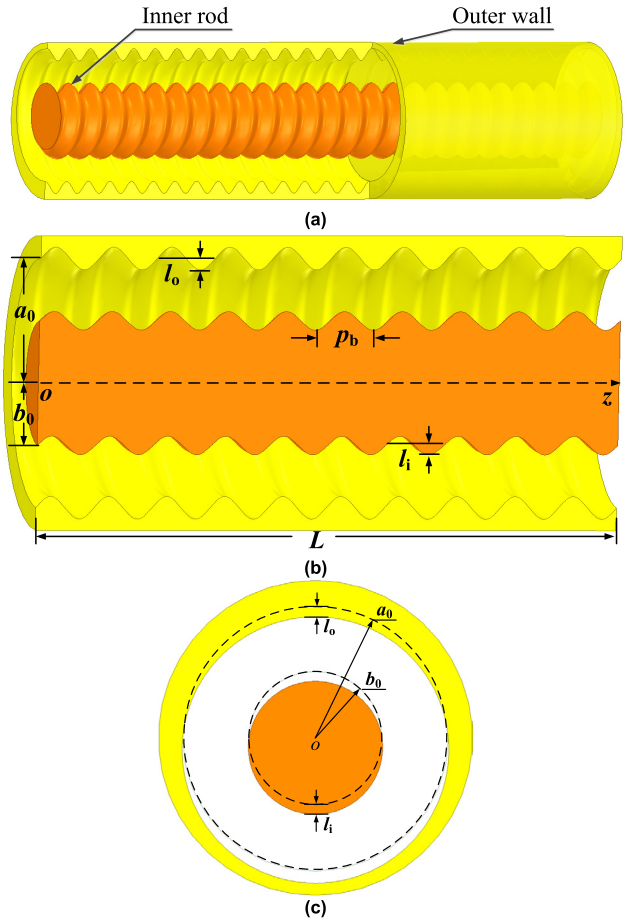

FIGURE 1. Schematic diagram (a) of a two-dimensional coaxial Bragg structure ($m_b = 1$) with helically corrugated conductors, where (b) is the longitudinal cross-section view and (c) is the transversal cross-section view at $z = 0$.

Fig. 1 shows the schematic and sectional views of a two-dimensional coaxial Bragg structure, constructed by inserting an outer corrugated inner rod into an inner corrugated hollow tube. The outer and inner conductors are corrugated cosinusoidally with the same length L, ripple period p_b, fold number m_b and initial corrugation phase $\varphi = 0$; the ripples on the surface of the outer and inner conductor have mean radius of a_0 and b_0, and constant amplitude l_o and l_i, respectively. As shown in Fig.2, supposing that the outer-wall ripples have an angular deviation of $\Delta\varphi$ with respect to the inner-rod ripples, the dependence of the outer-wall radius r_o and

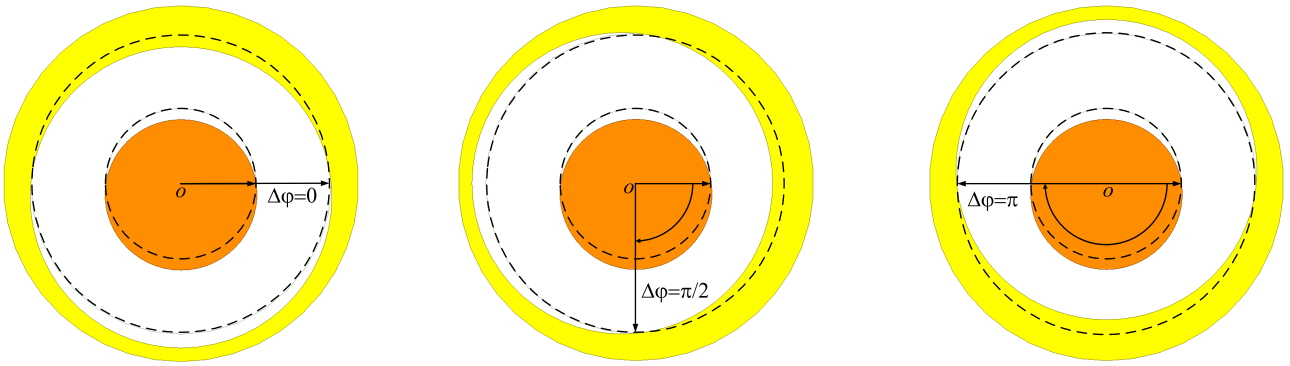

(a) $\Delta\varphi$=0 (b) $\Delta\varphi=\pi/2$ (c) $\Delta\varphi=\pi$

FIGURE 2. Transversal cross-section views of the entrance ($z = 0$) of a two-dimensional coaxial Bragg structure ($m_b = 1$) with the angular deviation $\Delta\varphi$ between the outer and inner corrugations equals to (a) 0, (b) $\pi/2$, and (c) π, respectively.

the inner-rod radius r_i on the longitudinal position z can be expressed by

$$r_o(\varphi, z) = a_0 + l_o \cos[m_b(\varphi + \Delta\varphi) + k_b z], \quad (1)$$

$$r_i(\varphi, z) = b_0 + l_i \cos(m_b\varphi + k_b z), \quad (2)$$

where $k_b = 2\pi/p_b$.

To highlight the theme of bandgap control, consider a two-dimensional coaxial Bragg structure with sufficiently large eigen-mode spectra intervals so that bandgaps associated with different coupled-mode combinations do not overlap with each other. Under this assumption, the incident wave of mode i will be strongly coupled with the backward wave of another mode k in the vicinity of Bragg resonance frequency, and the interaction of these two partial waves can be described by a pair of differential equations termed coupled-mode equations as [5], [11], [21], [22]

$$\frac{df_i^+}{dz} = -(\alpha_i + j\Delta_i)f_i^+ + jG_{ik}f_k^-, \quad (3)$$

$$\frac{df_k^-}{dz} = (\alpha_k + j\Delta_k)f_k^- - jG_{ik}^*f_i^+, \quad (4)$$

where

$$f_i^+ = A_i^+ e^{jk_b z/2}, \quad (5)$$

$$f_k^- = A_k^- e^{-jk_b z/2}. \quad (6)$$

A_i^+, α_i, $\Delta_i\left(=\beta_i - k_b/2\right)$ and β_i are the complex amplitude, the attenuation constant, the Bragg mismatch parameter and the axial wave number of the incident wave of mode i, respectively, while the subscript k represents the corresponding variation associated with the backward wave of mode k; G_{ik} and its complex conjugate G_{ik}^* denote the coupling coefficient between these two partial waves. The Bragg resonance frequency, i.e. the center frequency of the stopband, where the coherently coupling takes place, is determined by the following Bragg conditions:

$$\beta_i + \beta_k \approx k_b, \quad (7)$$

$$m_k - m_i = m_b. \quad (8)$$

The general solution of coupled-wave equations (3) and (4) can be expressed as

$$f_i^+(z) = \left[\left(\frac{1}{2} + \frac{\Delta\gamma}{2\Gamma}\right)f_i^+(0) - \frac{G_{ik}}{2\Gamma}f_k^-(0)\right]e^{-j\Gamma z}e^{-\bar{j}\bar{\gamma}z} + \left[\left(\frac{1}{2} - \frac{\Delta\gamma}{2\Gamma}\right)f_i^+(0) + \frac{G_{ik}}{2\Gamma}f_k^-(0)\right]e^{j\Gamma z}e^{-\bar{j}\bar{\gamma}z}, \quad (9)$$

$$f_k^-(z) = \left[\left(\frac{1}{2} - \frac{\Delta\gamma}{2\Gamma}\right)f_k^-(0) + \frac{G_{ik}^*}{2\Gamma}f_i^+(0)\right]e^{-j\Gamma z}e^{-\bar{j}\bar{\gamma}z} + \left[\left(\frac{1}{2} + \frac{\Delta\gamma}{2\Gamma}\right)f_k^-(0) - \frac{G_{ik}^*}{2\Gamma}f_i^+(0)\right]e^{j\Gamma z}e^{-\bar{j}\bar{\gamma}z}, \quad (10)$$

where

$$\Delta\gamma = \delta - \bar{j}\bar{\alpha}\left(\delta = \frac{(\beta_i + \beta_k - k_b)}{2}, \bar{\alpha} = \frac{\alpha_i + \alpha_k}{2}\right), \quad (11)$$

$$\bar{\gamma} = \Delta\beta - j\Delta\alpha\left(\Delta\beta = \frac{\beta_i - \beta_k}{2}, \Delta\alpha = \frac{\alpha_i - \alpha_k}{2}\right), \quad (12)$$

$$\Gamma = \sqrt{\Delta\gamma^2 - |G_{ik}|^2}. \quad (13)$$

$f_i^+(0)$ and $f_k^-(0)$ denote the amplitudes of f_i^+ and f_k^- at $z = 0$, respectively. Suppose that the incident wave of mode i is injected into the structure at $z = -L$ with a unit amplitude, and the output port of the structure at $z = 0$ is well matched to eliminate reflection, which can be expressed as

$$f_i^+(-L) = 1, \quad f_k^-(0) = 0. \quad (14)$$

By substituting (14) into the general solutions in (9), (10) and neglecting the loss of the corrugated surfaces, the reflectivity R and the transmission T of the structure in the vicinity of the Bragg resonance frequency can be obtained, which can be expressed as

$$R = \frac{f_k^-(-L)\cdot f_k^{-*}(-L)}{\left|f_i^+(-L)\right|^2} = \frac{\left(\frac{|G_{ik}|}{G}\right)^2 \sinh^2 GL}{\cosh^2 GL + \left(\frac{\delta}{G}\right)^2 \sinh^2 GL}, \quad (15)$$

$$T = \frac{f_i^+(0)\cdot f_i^{+*}(0)}{\left|f_i^+(-L)\right|^2} = \frac{1}{\cosh^2 GL + \frac{\delta^2}{G^2}\sinh^2 GL}, \tag{16}$$

where

$$G = \sqrt{|G_{ik}|^2 - \delta^2}, \tag{17}$$

sinh x and cosh$x$ are the hyperbolic sine and the hyperbolic cosine functions respectively. When the operating frequency f equals the Bragg resonance frequency f_0 that is determined by (7) and (8), there is $\delta = 0$ and $G = |G_{ik}|$, and the corresponding reflectivity R_0 and transmission T_0 can be rewritten as

$$R_0|_{f=f_0} = \tanh^2 |G_{ik}|\, L, \tag{18}$$

$$T_0|_{f=f_0} = \operatorname{sec h}^2 |G_{ik}|\, L. \tag{19}$$

Since the reflectivity/transmission at the Bragg resonance frequency is the key parameter that determines the width and amplitude of a bandgap, one can get a hint from (18) and (19) that bandgap control may be achieved if the coupling coefficient is tunable. According to the coupled-mode analytical model for two-dimensional coaxial Bragg structures established in [31], the coupling coefficient for the helical corrugations described by (1) and (2) can be denoted as

$$G_{ik} = \frac{\omega}{4}\left(l_o e^{-jm_b\Delta\varphi} p_{ik} - l_i q_{ik}\right), \tag{20}$$

where ω is the angular frequency; p_{ik} and q_{ik} are variables dependent on the types of mode i and mode k as well as the structure parameters, and their explicit formulas are given in [31]. Once the outer and inner conductors and their corrugated surfaces are processed, the corrugation amplitude l_o, l_i and the variables p_{ik}, q_{ik} are fixed with a constant value. However, from (20), one can find a special variable to manipulate the coupling coefficient G_{ik}, that is, the relative angular deviation $\Delta\varphi$, which is independent of the corrugation shape and the size of the outer and inner conductors. In particular, for a given combination of coupled modes, by properly setting the ratio b_0/a_0 and the corrugation amplitudes l_o and l_i, p_{ik} may be equal to q_{ik} in (20), then the coupling coefficient can be simplified as

$$G_{ik} = \mathcal{G}_0\left(1 - e^{jm_b\Delta\varphi}\right), \tag{21}$$

where

$$\mathcal{G}_0 = \frac{\omega}{4} l_o p_{ik} e^{-jm_b\Delta\varphi}. \tag{22}$$

Then, substitute (21) into (18) and (19), which yields

$$\mathcal{R}_0|_{f=f_0} = \tanh^2\left(2\left|\mathcal{G}_0 \sin\left(\frac{m_b}{2}\Delta\varphi\right)\right| L\right), \tag{23}$$

$$\mathcal{T}_0|_{f=f_0} = \operatorname{sec h}^2\left(2\left|\mathcal{G}_0 \sin\left(\frac{m_b}{2}\Delta\varphi\right)\right| L\right). \tag{24}$$

Evidently, (15)–(24) demonstrate the possibility of controlling the reflection/transmission bandgap of two-dimensional coaxial Bragg structures by varying the relative angular shift $\Delta\varphi$ between the outer and inner corrugations. In practice, this control method can be realized by rotating one of the outer or inner conductors along the azimuthal direction while keeping the other conductor fixed, thus avoiding any need to reprocess the corrugated conductors.

III. BANDGAP CONTROL IN TWO EXAMPLE STRUCTURES

To illustrate the feasibility of the bandgap control method, the transmission characteristics of two example structures with single bandgap and dual bandgap operation were investigated.

A. SINGLE BANDGAP OPERATION

First, consider a two-dimensional coaxial Bragg structure denoted as structure A. This structure had a mean outer-wall radius $a_0 = 11$ mm, a mean inner-rod radius $b_0 = 9$ mm and a total length $L = 80.2$ mm, and amplitude of the outer-wall and inner-rod ripples of $l_o = 0.15$ mm and $l_i = 0.12$ mm, respectively. The structure was injected with a basic TEM wave. Due to the cut-off of high-order modes, this incident wave can be coupled with the backward wave of only the $TE_{1,1}$ mode to form the required transmission bandgap within the Ka band. To ensure good synchronization of these two partial waves at the desired Bragg resonance frequency of 37.5 GHz, the axial period p_b and the fold number m_b of the structure were set to 4.01 mm and 1, respectively.

Based on the above structural configuration, the dependence of the magnitude of coupling coefficient $G_{\mathrm{TEM-TE1,1}}$ between incident and scattered waves on the angular deviation $\Delta\varphi$ was calculated and normalized by wave number $k_0 (= \omega\sqrt{\mu_0\varepsilon_0})$, where μ_0 and ε_0 are the permeability and permittivity of vacuum, respectively, and the results are shown in Fig.3. It is clear that, when the angular deviation $\Delta\varphi$ is 0 and 180°, the coupling coefficient reaches the minimum and maximum value respectively. Considering this feature, the transmission characteristics of structure A were further studied by varying the angular deviation $\Delta\varphi$ within the range of 0 to 180°. Fig. 4 shows the transmission rates of the incident wave at Bragg resonance frequency (37.5 GHz) versus angular deviation $\Delta\varphi$, where the solid lines denote the results calculated by using (24). For comparison, the S parameters of structure A were simulated by HFSS with an angular deviation step of 5°, where lambda refinement and surface approximation factors were set to 0.05 and 7 respectively to

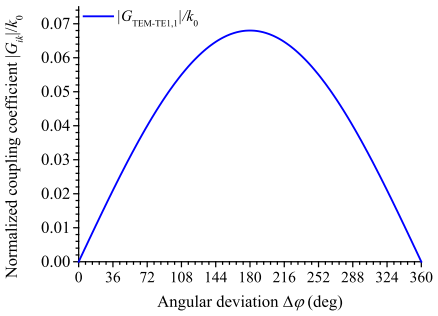

FIGURE 3. Dependence of the normalized magnitude of coupling coefficient between the incident TEM wave and the scattered $TE_{1,1}$ wave on the angular deviation $\Delta\varphi$ of structure A.

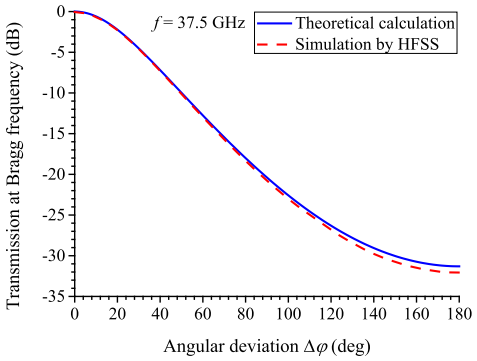

FIGURE 4. The transmission rates of the incident TEM wave at the Bragg frequency (37.5 GHz) versus the angular deviation $\Delta\varphi$ of structure A, where the solid line denotes theoretical results and the dashed line denotes the simulation results obtained by HFSS.

ensure high accuracy and convergence. The simulation model of structure A contained about 10 wavelengths of the incident TEM wave at 37.5 GHz in axial direction. These simulation results are shown in Fig.4 with a dashed line. Clearly, both the theoretical analysis and simulation results indicate the importance of the relative angular position between the outer and inner conductors for transmission at the Bragg resonance frequency, i.e., the center frequency of the bandgap.

Next, in order to illustrate the effect of angular deviation $\Delta\varphi$ on bandgap parameters, the frequency responses of transmission of structure A were analyzed using (16) as well as the frequency sweep tool of the HFSS. The results obtained by these two approaches are shown in Fig. 5 with solid lines and dashed lines respectively, where the angular deviation $\Delta\varphi$ is (a) 180°, (b) 90°, and (c) 0. It can be seen that, when the angular deviation $\Delta\varphi$ is 180°, owing to the maximum coupling coefficient, a sharp transmission bandgap appears in the vicinity of 37.5 GHz. The amplitude and width of this dominant transmission bandgap shrink with the reduction of $\Delta\varphi$ while the center frequency remains unchanged. Interestingly, as the outer and inner conductors had the same azimuthal position ($\Delta\varphi = 0$), the transmission bandgap almost disappeared in the operating frequency band. It should be pointed out that, since the ohmic loss of the corrugated surfaces was considered in the simulation, the transmission rates at the Bragg frequency obtained by HFSS were lower than those of theoretical analysis; meanwhile, the existence of ohmic loss reduced the frequency where the constructive interference between the incident wave and the scattered wave takes place, resulting in a downward shift of about 0.13 GHz of the transmission bandgap obtained by HFSS compared with theoretical results. However, principal consistency between the simulation results and theoretical calculations clearly confirms the validity of controlling the bandgap by changing the relative angular position of the inner and outer conductors.

B. DUAL BANDGAP OPERATION

The previous example demonstrates the bandgap control effect of angular deviation for a structure with single bandgap

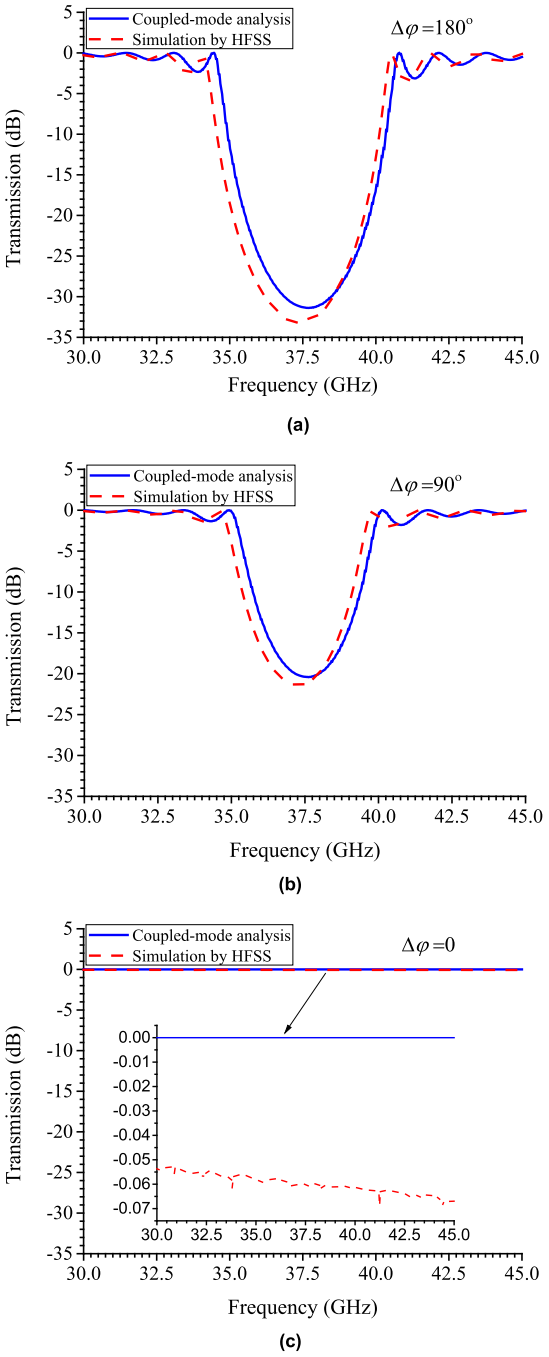

FIGURE 5. Transmission responses of structure A with an injection of TEM wave from 30GHz to 45GHz for the cases of the angular deviation $\Delta\varphi$ equals (a)180°, (b) 90°, and (c) 0, respectively, where the solid lines denote theoretical calculations by (16) and the dash lines denote the simulation results obtained by HFSS.

operation. By introducing additional backward coupling waves for an incident wave within the working frequency band, the proposed control method can achieve switching between single bandgap and dual bandgap operation for two dimensional coaxial Bragg structures. Consider another two-dimensional coaxial Bragg structure denoted as structure B, where the outer conductor had the same corrugation parameters as those of structure A, but for the inner conductor

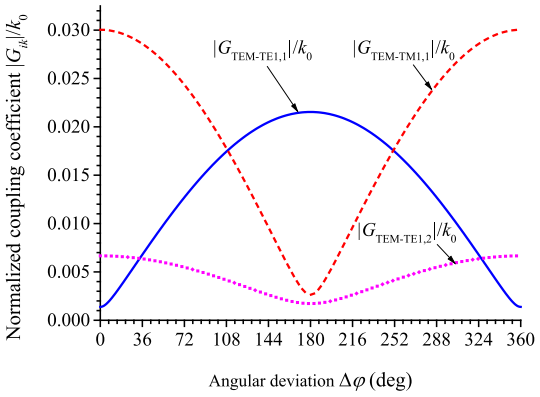

FIGURE 6. Dependence of the normalized magnitude of coupling coefficients associated with the coupled-mode combinations of TEM-$TE_{1,1}$ (solid line), TEM-$TM_{1,1}$ (dashed line) and TEM-$TE_{1,2}$ (dot line) on the angular deviation $\Delta\varphi$ of structure B.

the mean radius was reduced to 5.5 mm and the amplitude set to 0.09 mm. Both the outer and inner conductors were corrugated with the same axial period $p_b = 4.02$ mm, fold number $m_b = 1$ and length $L = 201$ mm.

Supposing that this structure was injected with a TEM wave, due to the reduction of the inner-rod radius, then besides the backward wave of $TE_{1,1}$ mode, the other two partial waves of higher-order modes $TE_{1,2}$ and $TM_{1,1}$ become traveling waves within the operating frequency range of 30 GHz–45 GHz and can be coupled with the incident wave. The dependence of normalized magnitude of coupling coefficients associated with coupled-mode combinations of TEM-$TE_{1,1}$, TEM-$TM_{1,1}$ and TEM-$TE_{1,2}$ on the angular deviation $\Delta\varphi$ are shown in Fig. 6. Evidently, the trend of changes in coupling coefficient $G_{\text{TEM}-\text{TE1,1}}$ with variation of $\Delta\varphi$ is opposite to those of changes in coupling coefficients $G_{\text{TEM}-\text{TM1,1}}$ and $G_{\text{TEM}-\text{TE1,1}}$. Thus it is possible to exert opposite control effects on the bandgaps associated with different coupled-mode combinations through varying the angular deviation $\Delta\varphi$.

Fig.7 shows the transmission responses of structure B within frequency of 30GHz–45GHz, obtained by multimode coupling analysis (solid lines) [31] and the frequency sweep tool of the HFSS (short dashed lines), where the angular deviation $\Delta\varphi$ equals (a) 0, (b) 180°, and (c) 117°. The simulation model of structure B was 2.5 times as long as that of structure A, which contained about 25 wavelengths of the incident TEM wave at 37.5 GHz in axial direction. As can be seen in Fig. 7, when $\Delta\varphi = 0$, there is one dominant transmission bandgap centered at 42.48 GHz; when $\Delta\varphi = 180°$, there is also one dominant transmission bandgap, but its center frequency is shifted to 37.52 GHz; when $\Delta\varphi = 117°$, two dominant transmission bandgaps appear with center frequencies of 37.52 GHz and 42.48 GHz, respectively. It is clear that, by changing the angular deviation, the number and location of the transmission bandgaps of a two dimensional coaxial Bragg structure can be manipulated.

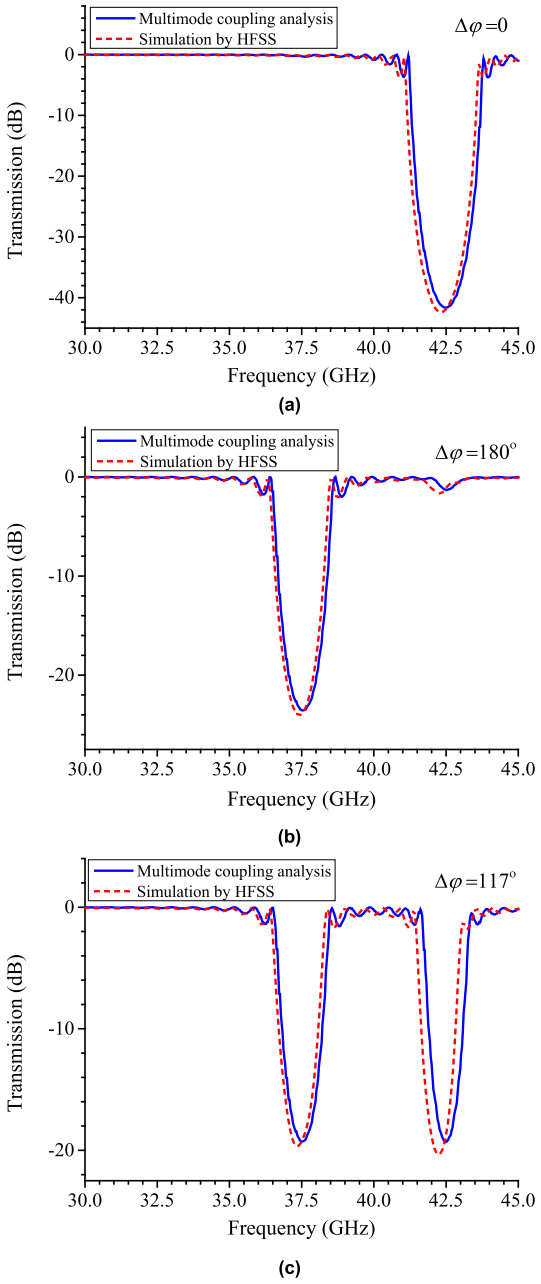

FIGURE 7. Transmission responses of structure B obtained by multimode coupling analysis (solid lines) and frequency sweep tool of HFSS (short dashed lines), where the incident wave is TEM from 30 GHz to 45 GHz, and the angular deviation $\Delta\varphi$ equals (a) 0, (b) 180°, and (c) 117°, respectively.

It is worthwhile to further discuss the physical mechanism behind the phenomena shown in Fig.7. According to the Bragg condition in (7) and (8), the Bragg resonance frequencies of coupled-mode combinations of TEM-$TE_{1,1}$, TEM-$TM_{1,1}$ and TEM-$TE_{1,2}$ are 37.52 GHz, 42.44 GHz and 42.72 GHz, respectively. Here, the latter two combinations have almost identical Bragg frequencies since the cutoff wave numbers of $TE_{1,2}$ and $TM_{1,1}$ are closed in structure B.

Then, if $\Delta\varphi = 0$, the coupling coefficients $G_{\text{TEM}-\text{TM1,1}}$ and $G_{\text{TEM}-\text{TE1,2}}$ reach their maximum value. The incident

TEM wave will be strongly scattered to the backward waves of $TM_{1,1}$ and $TE_{1,2}$ in the vicinity of the corresponding Bragg frequencies. The coupling of TEM-$TM_{1,1}$ and TEM-$TE_{1,2}$ will open only one transmission bandgap centered at 42.48 GHz due to the close Bragg frequencies of these two coupled-mode combinations.

By contrast, if $\Delta\varphi = 180°$, the minimum occurs for the coupling coefficients $G_{\mathrm{TEM-TM1,1}}$ and $G_{\mathrm{TEM-TE1,2}}$, thus the incident TEM wave will no longer be effectively coupled with the backward waves of $TM_{1,1}$ and $TE_{1,2}$, resulting in the closure of the original transmission bandgap located at 42.48 GHz. However, simultaneously, the coupling coefficient $G_{\mathrm{TEM-TE1,1}}$ will reach its maximum value, coherently scattering from the incident TEM wave to backward $TE_{1,1}$ generates another dominant bandgap centered at 37.52 GHz.

When $\Delta\varphi$ changes between 0 and 180°, the bandgaps centered at 37.52 GHz and 42.48 GHz display a dynamic tendency: as one falls, another rises. Specifically, as the $\Delta\varphi$ is set to a certain value, for example 117° in Fig. 5(c), two dominant bandgaps with nearly equal amplitude will be obtained.

Essentially, the change of coupling coefficients with the angular deviation $\Delta\varphi$ reflects the influence of boundary on mode coupling. Due to the synthesized effect of the outer and inner inhomogeneous boundaries, different coupled modes require different matched relative angular position of the outer and inner conductors to enhance coupling strength, thus the bandgaps at different positions in Fig.7 show different trends with variation of $\Delta\varphi$. On the other hand, according to (20), the coupling coefficient of a given coupled-mode combination is bound to get either a maximum or minimum value when $m_b\Delta\varphi = 0$ or π. This property may be related to the symmetry order of the periodic structures investigated in [32], that is, the structure possesses a higher symmetry if the relative phase between the outer and inner corrugations is equal to 0 or π. As demonstrated in [32], a higher symmetry is directly related to the absence of bandgap, resulting in the phenomena as shown in Fig. 7(a) and (b).

Finally, it should be noted that, although the above discussion of structure B focuses on control and switching between single bandgap and dual bandgaps, in fact, more bandgaps can be created if more partial waves of higher-order modes are introduced to be coupled with the incident wave under the conditions of reasonable structural parameters and higher upper operating frequency. Since the coupling coefficients associated with different coupled-mode combinations show different trends with the variation of angular deviation between the outer and inner corrugations, the proposed method of varying the angular position between the outer and inner conductors is still applicable for the manipulation of multiple bandgaps.

IV. CONCLUSION

The possibility of bandgap control of two-dimensional coaxial Bragg structures has been studied. Starting from coupled-mode equations, the principle as well as a theoretical model of bandgap control by varying the relative angular position between the outer and inner conductors was derived. Using coupled-mode theory and HFSS electromagnetic simulation software, the transmission characteristics of two example structures with a set of values of angular deviation between the outer and inner corrugations were investigated. By comparing the results, the following conclusions can be drawn:

1) Achieving bandgap control was based on the variable coupling coefficients, which were adjusted by varying the relative angular position between the inner and outer conductors. The other corrugation parameters of the inner and outer conductors did not need to be changed.

2) If only one backward wave could be coupled with the incident wave within the operating frequency range, a single transmission bandgap appeared and its amplitude and width could be controlled while its location remained fixed. Multiple transmission bandgaps could be generated by introducing additional coupled waves of higher-order modes for the incident wave, their number and location could be manipulated, and thus control and switching of the operating frequency band was achieved.

In summary, the bandgap of a two-dimensional coaxial Bragg structure can be manipulated with a fixed ripple shape of the inner and outer conductors. It facilitates the frequency switching of output radiation for microwave sources, and it also enables control and switching between single band and dual bands or even multi-band operation for other passive devices. The proposed bandgap control method therefore provides potential applications for two-dimensional coaxial Bragg structure in applications such as frequency-selective components of high-power microwave sources, and mode converters, filters or couplers for high-power microwave systems.

REFERENCES

[1] C. Elachi, "Waves in active and passive periodic structures: A review," *Proc. IEEE*, vol. 64, no. 12, pp. 1666–1698, Dec. 1976.

[2] A. Yariv and M. Nakamura, "Periodic structures for integrated optics," *IEEE J. Quantum Electron.*, vol. 13, no. 4, pp. 233–253, Apr. 1977.

[3] Z. Zhang and S. Satpathy, "Electromagnetic wave propagation in periodic structures: Bloch wave solution of Maxwell's equations," *Phys. Rev. Lett.*, vol. 65, no. 21, pp. 2650–2653, Nov. 1990.

[4] J. D. Joannopoulos, P. R. Villeneuve, and S. Fan, "Photonic crystals: Putting a new twist on light," *Nature*, vol. 386, no. 6621, pp. 143–149, Mar. 1997.

[5] C. K. Chong, D. B. Mcdermott, M. M. Razeghi, N. C. Luhmann, J. Pretterebner, D. Wagner, and M. Thumm, "Bragg reflectors," *IEEE Trans. Plasma Sci.*, vol. 20, no. 3, pp. 393–402, Jun. 1992.

[6] D. Wagner, W. Kasparek, F. Leuterer, F. Monaco, M. Munich, H. Schutz, T. Stange, J. Stober, and M. Thumm, "Bragg reflection band stop filter for ECE on Wega," *J. Infr., Millim., Terahertz Waves*, vol. 32, no. 12, pp. 1424–1433, 2011.

[7] M. Thumm, D. Wagner, E. D. Rijk, W. A. Bongers, W. Kasparek, F. Leuterer, A. Macor, J. Ansermet, F. Monaco, M. Munich, H. Schutz, J. Stober, H. V. D. Brand, and A. V. Bieren, "Multi-frequency notch filters and corrugated 200 to 400 GHz waveguide components manufactured by stacked ring technology," *Terahertz Sci. Technol.*, vol. 6, no. 4, pp. 212–222, 2013.

[8] Y. Guo, S. Kim, H. Gao, and G.-P. Li, "Compact high q configurable quint-band electromagnetic bandgap filter," *IEEE Access*, vol. 6, pp. 63703–63711, 2018.

[9] Y. Y. Danilov, M. I. Petelin, and S. Tantawi, "A coaxial 2D-periodic perforated directional coupler," *Radiophysics Quantum Electron.*, vol. 54, no. 11, pp. 731–736, Apr. 2012.
[10] D. Wu, F. Liu, X. Wang, H. Xu, L. Zhang, W. Xu, Y. Tang, and J. Wang, "The design of directional coupler for ECRH system," *IEEE Access*, vol. 5, pp. 6187–6191, 2017.
[11] V. Bratman, G. Denisov, N. Ginzburg, and M. Petelin, "FEL's with Bragg reflection resonators: Cyclotron autoresonance masers versus ubitrons," *IEEE J. Quantum Electron.*, vol. 19, no. 3, pp. 282–296, Mar. 1983.
[12] Y. Qian and T. Itoh, "Planar periodic structures for microwave and millimeter wave circuit applications," in *IEEE MTT-S Int. Microw. Symp. Dig.*, Anaheim, CA, USA, Jun. 1999, pp. 1533–1536.
[13] O. M. Haraz, A. Elboushi, S. A. Alshebeili, and A.-R. Sebak, "Dense dielectric patch array antenna with improved radiation characteristics using EBG ground structure and dielectric superstrate for future 5G cellular networks," *IEEE Access*, vol. 2, pp. 909–913, 2014.
[14] R. Halir, P. J. Bock, and P. Cheben, "Waveguide sub-wavelength structures: A review of principles and applications," *Laser Photon. Rev.*, vol. 9, no. 1, pp. 25–49, Sep. 2014.
[15] D. J. J. Hu, Z. Xu, and P. P. Shum, "Review on photonic crystal fibers with hybrid guiding mechanisms," *IEEE Access*, vol. 7, pp. 67469–67482, 2019.
[16] L. Kurra, M. P. Abegaonkar, A. Basu, and S. K. Koul, "Switchable and tunable notch in ultra-wideband filter using electromagnetic bandgap structure," *IEEE Microw. Wireless Compon. Lett.*, vol. 24, no. 12, pp. 839–841, Dec. 2014.
[17] D. Jiang, Y. Liu, X. Li, G. Wang, and Z. Zheng, "Tunable microwave bandpass filters with complementary split ring resonator and liquid crystal materials," *IEEE Access*, vol. 7, pp. 126265–126272, 2019.
[18] A. André and M. D. Lukin, "Manipulating light pulses via dynamically controlled photonic band gap," *Phys. Rev. Lett.*, vol. 89, no. 14, Sep. 2002.
[19] W. D. Cheng, S. P. Huang, D. S. Wu, X. D. Li, Y. Z. Lan, F. F. Li, J. Shen, H. Zhang, and Y. J. Gong, "Band-gap control optical Kerr effect and light self-focusing of semiconducting materials $Cd_xHg_{1--x}Ga_2S_4$," *Appl. Phys. Lett.*, vol. 87, no. 9, Sep. 2005, Art. no. 141905.
[20] J. A. Reyes and A. Lakhtakia, "Electrically controlled optical bandgap in a structurally chiral material," *Opt. Commun.*, vol. 259, no. 1, pp. 164–173, Mar. 2006.
[21] G. G. Denisov, V. L. Bratman, A. D. R. Phelps, and S. V. Samsonov, "Gyro-TWT with a helical operating waveguide: New possibilities to enhance efficiency and frequency bandwidth," *IEEE Trans. Plasma Sci.*, vol. 26, no. 3, pp. 508–518, Jun. 1998.
[22] M. I. Fuks, M. B. Goikhman, N. F. Kovalev, A. V. Palitsin, and E. Schamiloglu, "Waveguide resonators with combined Bragg reflectors," *IEEE Trans. Plasma Sci.*, vol. 32, no. 3, pp. 1323–1333, Jun. 2004.
[23] W. He, A. W. Cross, A. D. R. Phelps, K. Ronald, C. G. Whyte, S. V. Samsonov, V. L. Bratman, and G. G. Denisov, "Theory and simulations of a gyrotron backward wave oscillator using a helical interaction waveguide," *Appl. Phys. Lett.*, vol. 89, no. 9, Aug. 2006, Art. no. 091504.
[24] S. V. Samsonov, A. D. R. Phelps, V. L. Bratman, G. Burt, G. G. Denisov, A. W. Cross, K. Ronald, W. He, and H. Yin, "Compression of frequency-modulated pulses using helically corrugated waveguides and its potential for generating multigigawatt RF radiation," *Phys. Rev. Lett.*, vol. 92, no. 11, Mar. 2004.
[25] L. Zhang, W. He, K. Ronald, A. D. R. Phelps, C. G. Whyte, C. W. Robertson, A. R. Young, C. R. Donaldson, and A. W. Cross, "Multi-mode coupling wave theory for helically corrugated waveguide," *IEEE Trans. Microw. Theory Techn.*, vol. 60, no. 1, pp. 1–7, Jan. 2012.
[26] A. W. Cross, I. V. Konoplev, A. D. R. Phelps, and K. Ronald, "Studies of surface two-dimensional photonic band-gap structures," *J. Appl. Phys.*, vol. 93, no. 4, pp. 2208–2218, Feb. 2003.
[27] J. J. Barroso and J. P. L. Neto, "Design of coaxial Bragg reflectors," *IEEE Trans. Plasma Sci.*, vol. 34, no. 3, pp. 666–672, Jun. 2006.
[28] I. V. Konoplev, P. McGrane, A. W. Cross, K. Ronald, and A. D. R. Phelps, "Wave interference and band gap control in multiconductor one-dimensional Bragg structures," *J. Appl. Phys.*, vol. 97, no. 7, Apr. 2005, Art. no. 073101.
[29] N. S. Ginzburg, E. V. Ilyakov, I. S. Kulagin, N. Y. Peskov, R. M. Rozental, A. S. Sergeev, V. Y. Zaslavsky, and I. V. Zheleznov, "Synchronization of radiation in an oversized coaxial ka-band backward wave oscillator using two-dimensional Bragg structure," *Phys. Rev. Special Topics-Accel. Beams*, vol. 18, no. 12, pp. 85–129, Dec. 2015.
[30] Y.-X. Lai, S.-C. Zhang, and H.-B. Zhang, "A coaxial Bragg reflector for cyclotron autoresonance maser oscillators," *IEEE Microw. Wireless Compon. Lett.*, vol. 17, no. 5, pp. 328–330, May 2007.
[31] Y.-X. Lai, X.-M. Jiang, S.-J. Wang, and T.-J. Liu, "Coupled-mode analysis for two-dimensional coaxial Bragg structures with helical ripples," *Phys. Plasmas*, vol. 25, no. 9, Sep. 2018, Art. no. 093104.
[32] O. Dahlberg, F. Ghasemifard, G. Valerio, and O. Quevedo-Teruel, "Propagation characteristics of periodic structures possessing twist and polar glide symmetries," *EPJ Appl. Metamater.*, vol. 6, no. 14, pp. 1–6, 2019.

YING-XIN LAI (Member, IEEE) received the B.S. and Ph.D. degrees from Southwest Jiaotong University (SWJTU), Chengdu, China, in July 2003 and December 2008, respectively.

He is currently an Associate Professor with the School of Electronic Engineering and Intelligentization, Dongguan University of Technology (DGUT), Dongguan, China. His research interests include high-power microwave sources, antennas, millimeter passive devices, and microwave-photonic sensors.

XIAO-MIN JIANG received the B.Eng. degree in electronic information science and technology from Southwest Jiaotong University, Chengdu, China, in 2008, and the Ph.D. degree in electromagnetic fields and microwave technology from Peking University, Beijing, China, in 2013.

He is currently a Lecturer with the Dongguan University of Technology. His main research interests include radar automatic target recognition (RATR), radar signal processing, and pattern recognition.

FANG-YUAN CHEN received the Ph.D. degree from Sichuan University, China, in 2016.

From 2013 to 2015, he was a Visiting Ph.D. Student with Cornell University, USA. From 2017 to 2019, he was a Research Engineer with Radio Frequency System-Nokia Bell Company. He is currently the Vice Chief Engineer of Jinyichang Science and Technology Company Ltd., China. His research interests include antenna theory and design, microwave circuit, multiphysics computation, and automatic drive.

Dr. Chen is a member of Applied Computational Electromagnetics Society, and of peer reviewers of multiple international journals.

JIAN LI (Member, IEEE) received the B.S., M.S., and Ph.D. degrees in communication and information system from the University of Electronic Science and Technology of China, Chengdu, China, in 2007, 2010, and 2015, respectively.

Since 2017, he has been an Associate Professor with the School of Communication and Information Engineering, University of Electronic Science and Technology of China. He was a Visiting Scholar with the Center for Computational Electromagnetics, Department of Electrical and Computer Engineering, University of Illinois at Urbana-Champaign, Urbana, IL, USA, from 2016 to 2017. He has authored or coauthored over 80 papers in refereed journals and conferences. His current research interests include RFID, the IoT, passive communication systems, bioelectromagnetics, integrated circuits and systems, and electromagnetic metamaterials and its applications.

TAI-JUN LIU (Senior Member, IEEE) received the B.S. degree in applied physics from the China University of Petroleum, Qingdao, China, in 1986, the M.Eng. degree in microwave technology from the University of Electronic Science and Technology of China, Chengdu, China, in 1989, and the Ph.D. degree from the École Polytechnique de Montréal, University of Montreal, Montreal, QC, Canada, in 2006.

He is currently a Professor with the Faculty of Electrical Engineering and Computer Science, Ningbo University, Ningbo, China. His current research interests include nonlinear modeling and linearization of wideband transmitters/power amplifiers, and the design of ultra-linear high-efficiency intelligent power amplifiers for broadband wireless and satellite communication systems.